ADVANCED FUNCTIONAL MATERIALS
www.afm-journal.de

www.MaterialsViews.com

A Novel $MoSe_2$–Reduced Graphene Oxide/Polyimide Composite Film for Applications in Electrocatalysis and Photoelectrocatalysis Hydrogen Evolution

*Lingpu Jia, Xiao Sun, Yimin Jiang, Shenjiao Yu, and Chunming Wang**

Promising catalytic activity of $MoSe_2$ in the hydrogen evolution reaction (HER) is synthesized on a new reduced graphene oxide/polyimide (rGO/PI) substrate by a simple electrochemical method. The $MoSe_2$ nanoparticles have excellent photo-responsive properties; the potential difference could reach 0.45 V with the photo-responsive time just 0.6 s. Furthermore, $MoSe_2$ thin film exhibits superior catalytic activity in the hydrogen evolution reaction (HER). It has a greater cathode current at more positive potential compared to other $MoSe_2$ and MoS_2, and the efficiency of H_2 evolution is strongly influenced by illumination; this suggests that $MoSe_2$ composite film has good photoelectrocatalysis properties for hydrogen evolution. Besides, both dark and illumination $MoSe_2$ films exhibit extremely high stability in acidic solution as the HER catalytic activity shows no degradation after 100 cycles for two hours. All results indicate that $MoSe_2$–rGO/PI composite film has potential to be a better catalyst for HER.

1. Introduction

Hydrogen production from water splitting has attracted growing attention for fulfilling the global energy demand and for tackling the environmental issues.[1,2] While Pt and its alloys are the best catalysts for the hydrogen evolution reaction (HER) in acidic media, but their low abundance and high cost prevent the massive deployment of these materials for hydrogen production. Therefore, it is necessary to investigate other types materials that can mimic the performance of Pt for the HER.[3–5] $MoSe_2$ is a semiconductor whose structure is similar to graphene, it is endowed with a bang gap of 1.7–1.9 eV and good semiconductor properties.[6–8] To date, several $MoSe_2$ nanostructures were published that showed an excellent HER performance. However, some of these approaches usually need either high temperature or high pressure, long reaction time or special devices, while some require toxic reagents.[9–12] As an alternative approach, electrochemical deposition can commendably control film ingredients, thickness, purity and uniformity; it is a technique with many advantages including simple equipment, considerable low temperature, controllable conditions and environmentally friendly.[13–17]

Although the HER performance of $MoSe_2$ has been studied, the semiconductor properties are underutilized. $MoSe_2$ has good photoelectric property,[18] what if the HER performance combines with photoelectric property, the $MoSe_2$ will be utilized fully. In our work, $MoSe_2$ is fabricated on a new rGO/PI composite substrate by electrochemical deposition. rGO/PI film as working electrode is chosen by its advantages; such as flexible, light, excellent mechanical property, thermal stability, dimensional stability and so on. Besides, the rGO/PI membrane can withstand heat and cold over a wide temperature range of –200 to 300 °C.[19–21] Photoelectrochemical water splitting is emerging as a promising clean technique for the synthesis of H_2 gas, which could be used as a clean and renewable energy source. By a series of study, it is found that $MoSe_2$ exhibits superior electrocatalytic and photoelectrocatalytic activity in the HER, because the deposition can generate very high photocurrent for hydrogen evolution under irradiation. Besides, it has a greater cathode current at more positive potential comparing with other materials. The photoelectric property also exhibits excellent reversibility and stability. All results indicate that the p-type $MoSe_2$– rGO/PI composite film is promising to be used for solar-driven hydrogen evolution.

2. Result and Discussion

2.1. Electrochemical Characteristics

Cyclic voltammetry is the best tool to investigate electrochemical reaction in precursor solutions. **Figure 1**A shows the CVs of Na_2MoO_4 measured at the rGO/PI membrane electrode, the cathodic current began to increase gradually at –0.45 V, and an obvious peak was obtained at -0.8V, it can be ascribed to the reduction of MoO_4^{2-}. The electrochemical behavior of Se was also studied, the reduction potential is between –0.4 and

L. P. Jia, X. Sun, Y. M. Jiang, S. J. Yu,
Prof. C. M. Wang
Department of Chemistry
and Chemical Engineering
Lanzhou University
222 Tianshui road, Lanzhou of Gansu province
730000, China
E-mail: wangcm@lzu.edu.cn

DOI: 10.1002/adfm.201401814

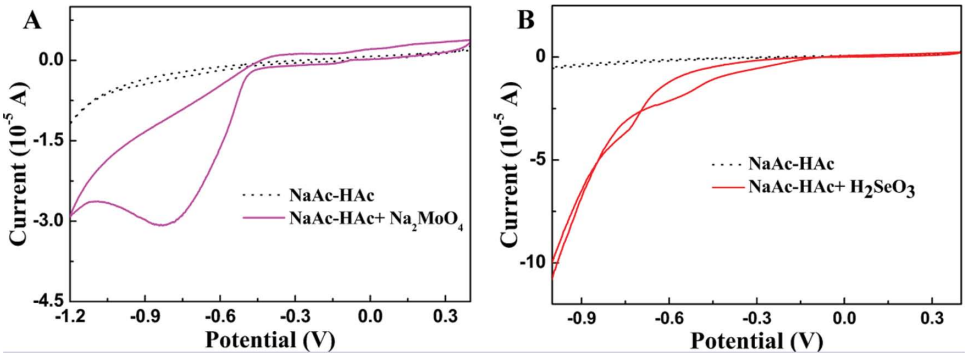

Figure 1. CV measured on the rGO/PI membrane electrode corresponding to A) 0.2 M NaAc-HAc buffered solution (PH = 3.6) and 5 mM Na_2MoO_4; B) 0.2 M NaAc-HAc buffered solution and 5 mM H_2SeO_3.

–0.7 V, as shown in Figure 1B. Besides, in order to optimize the deposition conditions for $MoSe_2$, the effect of deposition potentials and concentrations were investigated. At last the electrodeposition conditions for $MoSe_2$ are 0.04 M Na_2MoO_4, 0.02 M H_2SeO_3, and 0.2 M NaAc–HAc buffered solution (PH = 3.6) at –0.6 V.

2.2. Structure and Morphology

The morphologies of the obtained samples were investigated in detail by SEM. **Figure 2**A–D show the SEM images of samples obtained at 5, 10, 20, and 30 min. The morphologies of products are all nanoparticles, which indicated that the morphology of product would not change with different time, it just increased the amount. The diameters of these $MoSe_2$ particles are estimated to be approximately 30–50 nm because the size of 30–40 and 40–50 nm particles are the great mass of them corresponding to 59.8% and 32.6% respectively, as is shown in Figure 2E; the 20–30 and 50–60 nm particles were just few. Figure 2F shows the ratio of $MoSe_2$, it was calculated to be 1:2, in agreement with the stoichiometric ratio. Besides, the C and O peaks were ascribed to the substrate rGO/PI.

The TEM image in **Figure 3**A shows the as-formed $MoSe_2$ is nanoparticles with various sizes, and the size range is according with the statistics in Figure 2E. The HRTEM image (Figure 3B) reveals clearly lattice fringe of $MoSe_2$, and the lattice stripe spacing along the growth axis is 0.33 nm; corresponding to the interplanar distance of (004) diffraction crystal. Figure 3C shows that $MoSe_2$ is a polycrystalline nature. To confirm the crystalline structure of the $MoSe_2$ film, the sample was researched by XRD, as shown Figure 3D. There were three obvious strong peaks, all recorded diffraction peaks could be easily indicated to the crystal planes of (004) (012) and (104). The crystal plane (004) can be indexed to the crystal phase of $MoSe_2$ (JCPDS: 29–0914), and the others were ascribed to the phase (JCPDS: 20–0757). Besides, the XRD result also illustrates that the $MoSe_2$ is a polycrystalline material. The Raman spectrum of $MoSe_2$ was shown in Figure 3E, the A_{1g} was out-of-plane mode and E^1_{2g} was in-plane mode

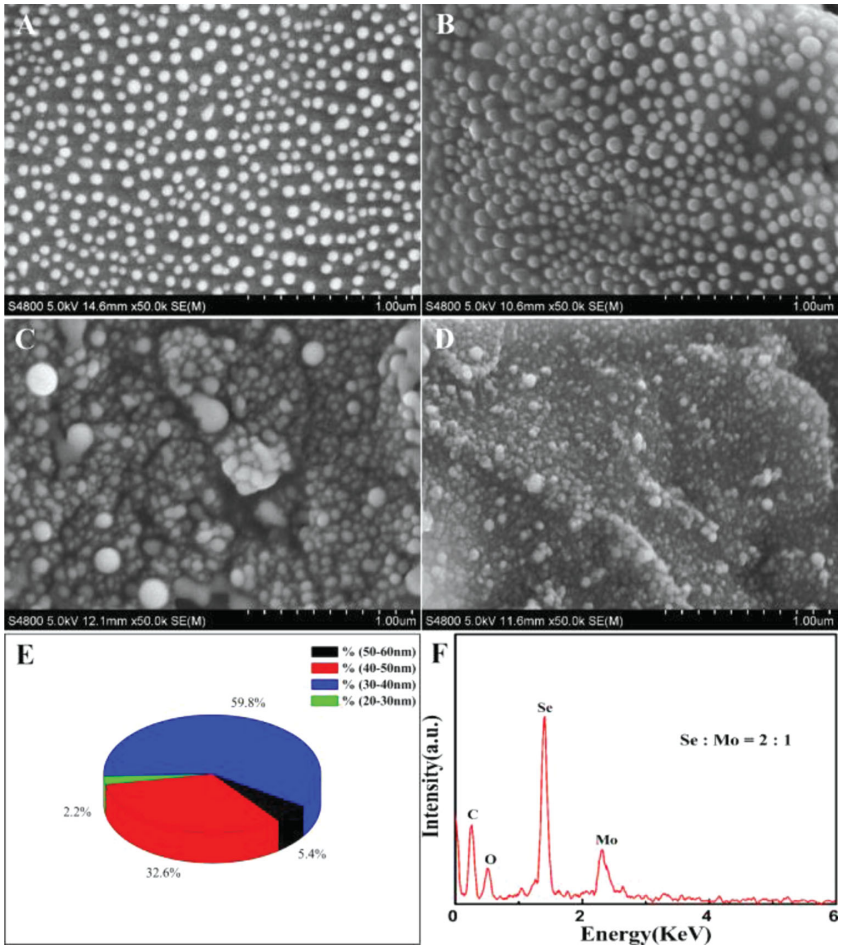

Figure 2. SEM images of $MoSe_2$ nanoparticles on substrate rGO/PI: A–D) SEM images of $MoSe_2$ with elctrodeposition 5, 10, 20, and 30 min; E) the distribution of $MoSe_2$ nanoparticles size; F) EDS of $MoSe_2$.

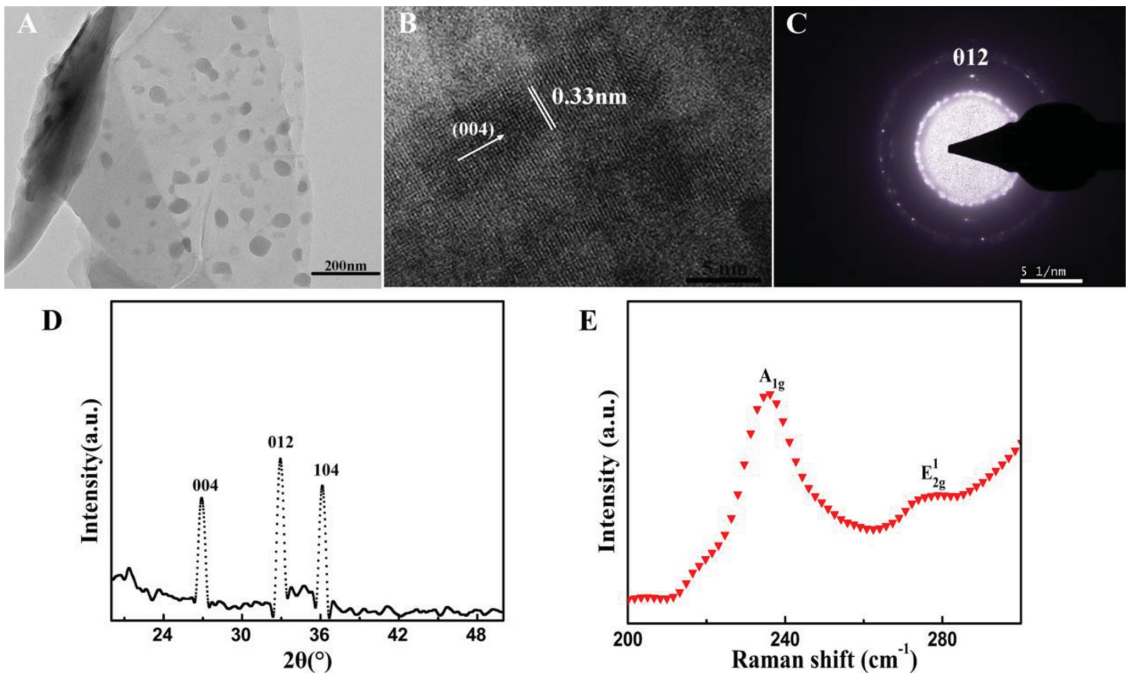

Figure 3. Structure of $MoSe_2$. A) TEM image of $MoSe_2$ nanoparticles; B,C) HRTEM and selected area electron diffraction images; D,E) XRD pattern and Raman spectrum.

with the former being at a higher frequency than the latter. The nanoparticles showed characteristic A_{1g} and E^1_{2g} Raman modes located at 236 cm^{-1} and 278 cm^{-1}, respectively.

Chemical compositions of these materials were further investigated by X-ray photoelectron spectroscopy (XPS) analysis (**Figure 4**). The binding energies of Mo $3d_{5/2}$ and Mo$3d_{3/2}$ were 229 and 232 eV in Figure 4B, respectively; revealing the +4 oxidation chemical state of Mo.[22–24] Se 3d XPS analysis showed two peaks for $3d_{5/2}$ at 54.5 eV and $3d_{3/2}$ at 55.4 eV, as shown in Figure 4C; indicating the oxidation state of –2 for Se in material.[25,26] Quantitative elemental analysis from XPS peaks integration showed 34.2% Mo and 65.8% Se; which confirms that deposition ratio of Mo: Se is about 1 : 2, it confirmed each other with EDS result. All the conclusions demonstrate the deposition on rGO/PI is $MoSe_2$.

2.3. Photoelectric Property

In order to study the photoelectric property of $MoSe_2$, OCP and amperomertric methods (*i–t*) were performed in 0.2 M NaAc-HAc buffered solution (PH = 3.6) during sequential darkness and illumination. OCP was measured with the xenon lamp time interval 200 s that turned on and turned off as shown in **Figure 5**A. Remarkable photoelectric response was observed from the on/off light cycles. V_{ocp} stayed at a lower level with light off and increased quickly under irradiation, which indicated $MoSe_2$ nanoparticles is p-type conductive material, and the potential difference can reach 0.45 V. The i–t study of $MoSe_2$ was performed with on–off irradiation cycles interval 50 s at –0.3 V. As seen in Figure 5B, the current difference induced by irradiation is 80 uA/cm^2 for $MoSe_2$. Figure 5C–D show the photo-responsive characteristics of $MoSe_2$. When the light was turned on, the photocurrent increased rapidly in 0.6 s. A spike value of photocurrent can be observed because of the transient effect in power excitation, whereafter the photocurrent achieved a steady value rapidly; after switching off the light, the photocurrent reduced quickly in 0.5 s and recovered to the original current value; these were accorded with the OCP result. The change regular of photoelectric phenomenon for $MoSe_2$ is because the electron of valence band will jump into conduction band as soon as photon energy is greater than or equal to the band gap

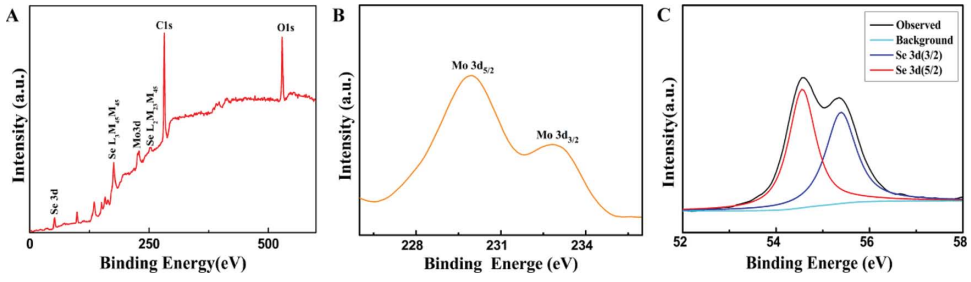

Figure 4. XPS core level spectra of $MoSe_2$: A) Survey spectra; B) High resolution Mo 3d spectra; C) High resolution Se 3d spectra.

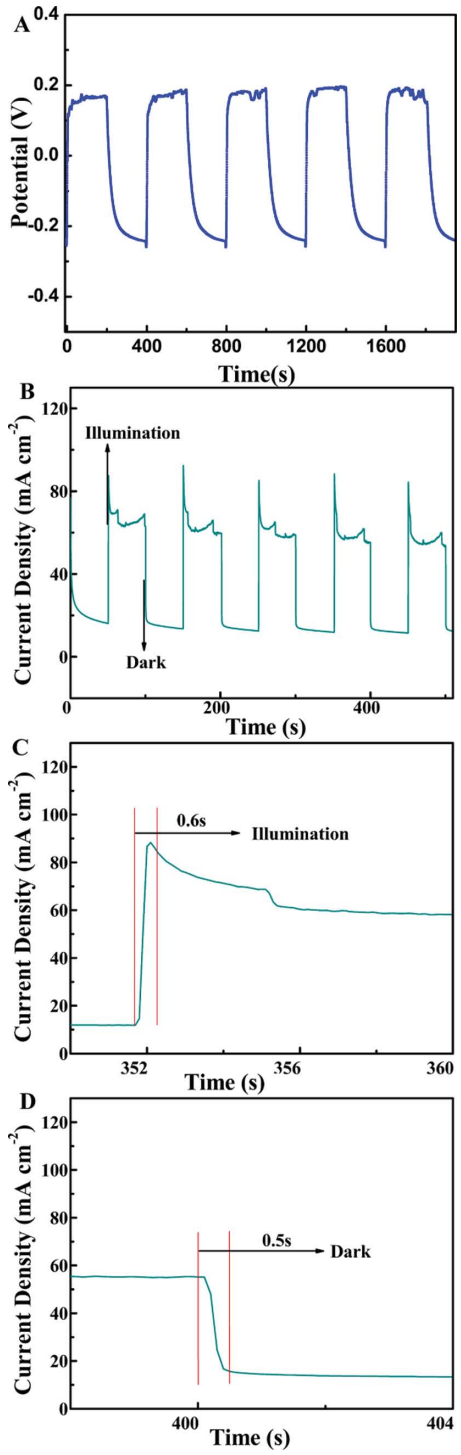

Figure 5. A) OCP vs time of $MoSe_2$. B) *I–V* curves of the $MoSe_2$ measured in the dark and under illumination; C,D) photocurrent–time curves of the photosensitiveness.

energy of the semiconductor under illuminated, but p-type semiconductor compound has more electro holes than electrons, at this moment, electro holes would act as conductive task.[27] After scores of cycles, the photocurrent can be still changed distinctly with repeatedly turning the xenon lamp on and off; demonstrating that $MoSe_2$ composite membrane has excellent reversibility and stability.

2.4. Electrocatalysis H_2 Evolution Activity

To evaluate the catalytic activity of $MoSe_2$ over substrate rGO/PI, the catalytic activity for H_2 was examined in 0.5 M H_2SO_4 with the scan rate of 50 mV s^{-1}. Linear sweep voltammetry (LSV) was used to determine the kinetic activity of the films. **Figure 6**A shows the results of LSV about bare substrate and $MoSe_2$ electrodeposited for 5min. From the polarization measurements, the current density of substrate rGO/PI almost remain unchanged in the potential range; but the cathodic current of $MoSe_2$ began to increase gradually at –0.25 V versus SCE and had an obvious increase at –0.45 V, illustrating $MoSe_2$ displays excellent responsive for H^+. Figure 6B shows polarization curves of the $MoSe_2$ with deposition time increasing from 5 to 40 min. As the deposition time increases during 5 and 35 min, the overpotential decreases. However, when time extented to 40 min, the catalytic activity almost kept stable even reduced. So the best elcterodeposition time is 35 min for $MoSe_2$. The $MoSe_2$ (35 min) film displays an onset potential for hydrogen evolution with high catalytic current densities of 3.1 mA/cm^2 at –0.3 V, and the maximum current density of 29 mA/cm^2 was obtained at –0.8 V. Compared to other $MoSe_2$ and MoS_2 in these literatures,[9,10,28–30] It is found the $MoSe_2$ (35 min) has even more current densities at low potentials, as **Table 1**. The potentials in Table 1 are corresponded to normal hydrogen electrode potentials. The potential was converted to the NHE electrode by

$$E(\mathrm{NHE}) = E(\mathrm{Hg/Hgcl_2}) + 0.251\mathrm{V}$$

The $E(\mathrm{Hg/Hgcl_2})$ is 0.251 V at 15 °C.

2.5. Photoelectrocatalysis H_2 Evolution Activity

The photoelectric hydrogen evolution of $MoSe_2$ was investigated under xenon lamp; all measure process was under illumination. The investigation conditions are the same as the previous hydrogen evolution. The catalytic current increased obviously by the light enhanced at the same potential from **Figure 7**. For example, the cathode current 10.9 mA cm^{-2} of –0.6 V increased to 14.5 mA cm^{-2} with 400 W illumination, illustrating irradiation could effectively promote HER for $MoSe_2$. The unique property of p-type $MoSe_2$-rGO/PI composite film makes it promising to be used for solar-driven hydrogen evolution.[31–33]

Figure 8A shows the photocatalysis principle diagram for HER. $MoSe_2$ is a p-type semiconductor, the H^+ will capture the electron that valence band jumped into conduction band as soon as the semiconductor is illuminated, so irradiation promote hydrogen evolution for $MoSe_2$.[34–37] Figure 8B is the phenomenon during hydrogen evolution reaction process, the solution belches out a lot of bubbles, it reflects factually the excellent catalytic activity of $MoSe_2$.

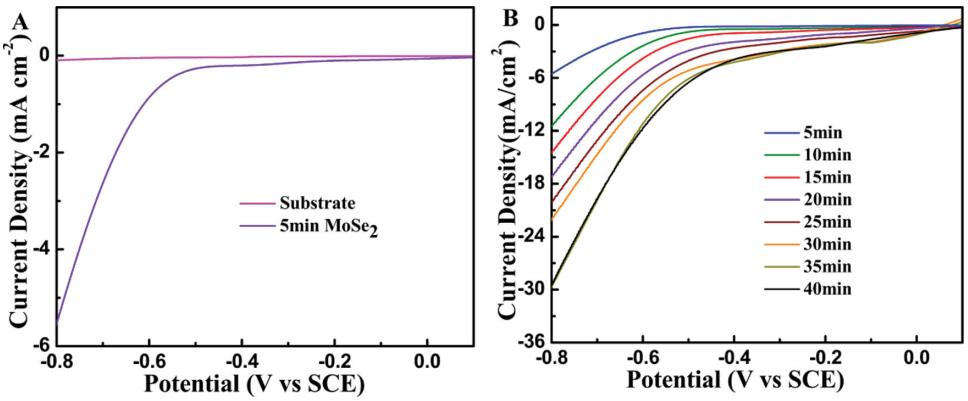

Figure 6. Hydrogen evolution reaction (HER) in 0.5 M H_2SO_4 at the scan rate of 50 mV s^{-1}; A) Polarization curves of $MoSe_2$ film (5 min) as well as blank rGO/PI substrate showing H_2 evolution; B) polarization curves of the $MoSe_2$ with increasing deposition time from 5 to 40 min.

2.6. The Stability and Tafel Slope

Another important criterion for a good electrocatalyst is high durability. The as-grown catalyst was cycled by taking continuous LSV between −1.0 and 0.1 V for $MoSe_2$ versus SCE. The polarization curves before and after cycling were recorded with a rate of 50 mV s^{-1} about two hours. **Figure 9**A,B show the stability under dark, polarization curves after the 100 cycles diverged from the curve of the first cycle with small increase of cathodic current, as shown in Figure 8B. The curves of Figure 9C,D were obtained under illumination, the catalyst activities are improved markedly, and along with the increasing of times, the cathodic currents increased a little every other 50 cycles. These results confirmed the extremely high stabilitiy of $MoSe_2$ whether dark or irradiation. So good stability of $MoSe_2$-rGO/PI composite membrane demonstrates further it is a good material for solar-driven hydrogen evolution.

The stability of $MoSe_2$-rGO/PI composite membrane was investigated further with current density vs time curve, the electrode was polarized at a potential V = −0.6 V. As shown in **Figure 10**A. The stability of the cathodic photocurrent seems surprising since it hardly decreased; both in dark and illumination the substrate emerged high stability and sufficient cathodic current density, which is in accord with previous result, and they are mutual corroboration. The Tafel slope is an inherent property of the catalyst that is determined by the rate-limiting step of the HER. The overpotential η(V) observed during an experiment is given by $\eta = a + b \log |j|$; where a (mV) is the Tafel constant, j (mA cm^{-2}) is the current density and b is the Tafel slope. The linear portions of the Tafel plots (Figure 10B) were fitted to the Tafel equation yielding Tafel slope of 82 mV per dec. According to the three possible reaction steps that have been suggested for the HER in acidic media;[38–40] in this work, it seems that the free energy barrier of the discharge step is reduced to be comparable with that of the following desorption or discharge step, resulting in the slope of 82 mV dec^{-1}. A small Tafel slope is desired for practical application of HER catalysts, and the Tafel slopes of $MoSe_2$ nanoparticles is smaller than other $MoSe_2$ prepared in these literatures,[9,41] The plausible reasons is: 1) the $MoSe_2$ is prepared electrodeposition, the small nanoparticles are more beneficial to the hydrogen evolution; 2) the new substrate rGO/PI composite membrane possesses more superficial area compared to basal plane. These results indicate the

Table 1. Comparison the current density at the same potentials based on rGO/PI–$MoSe_2$ nanoparticles with other hydrogen evolution materials. The potentials correspond to normal hydrogen electrode potentials.

Materials	J (−0.1 V) mA cm^{-2}	J (−0.2 V) mA cm^{-2}	J (−0.3 V) mA cm^{-2}	Ref.
MoS_2	0.1	0.5	2	[9]
$MoSe_2$	0.1	0.8	2	[9]
$MoSe_2$	<1	3	15	[10]
MoS_2	<1	<1	3	[28]
MoS_2/RGO	<1.5	30	–	[29]
MoS_2	<1	<1	20	[30]
$MoSe_2$	3.6	4.9	7.9	This work

J is the current density.

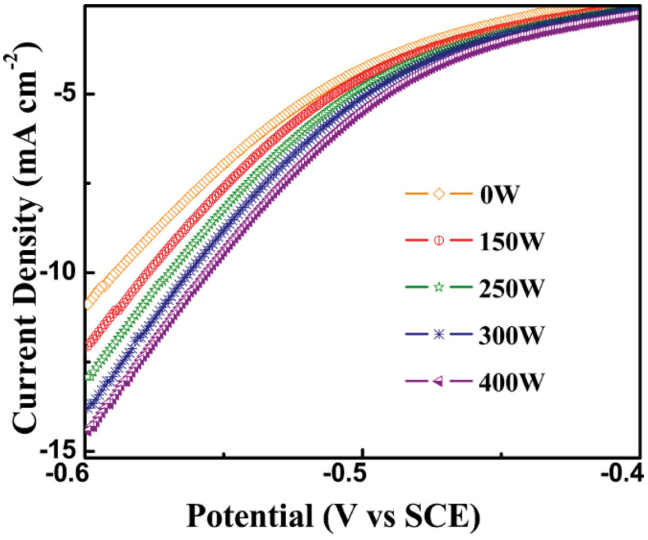

Figure 7. The HER catalytic activity of $MoSe_2$ composite membrane varied with illumination intensity.

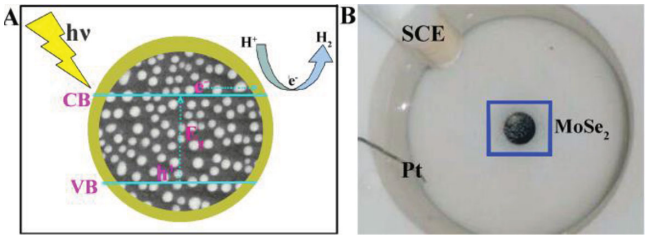

Figure 8. A) photocatalysis principle diagram of p-type semiconductor for HER; B) the phenomenon of $MoSe_2$– rGO/PI film for hydrogen evolution reaction.

$MoSe_2$–rGO/PI composite film is a promising candidate for HER in photoelectrochemical cells.

3. Conclusion

In conclusion, we have first synthesized $MoSe_2$ nanoparticles on rGO/PI substrate by a simple electrodeposition method. The resulting product exhibited superior photoelectric property and HER activity. Although the $MoSe_2$ is still a little worse than the best catalytic activity, it has an advantage that greater cathode current appears at more positive potential compared to other $MoSe_2$ and MoS_2 materials. The hydrogen evolution reaction is combined with irradiation finding that the catalytic activity of $MoSe_2$ nanoparticles enhanced. Besides, both dark and irradiation $MoSe_2$ film exhibits extremely high stability in acidic solution, all results point out that the $MoSe_2$ composite film has potential to be a better catalyst for HER and solar-driven hydrogen evolution.

4. Experimental Section

Materials and Instruments: All electrochemical experiments were performed using a CHI 832 Instruments (CH Instrument, USA). The surface morphology was observed through a field-emission scanning electron microscope (FE-SEM) (Hitachi S-4800, Japan). The crystalline structure was determined by X-ray diffraction (XRD) (RigakuD/max-2400) and X-ray photoelectron spectroscopy (XPS) was used to analyze the chemical environment of elements present in $MoSe_2$. Transmission electron microscopy (TEM) images, high-resolution transmission electron microscopy (HRTEM) images were taken with an analytical TEM apparatus from FEI Tecnai G^2 F30 TEM. The photo electrochemical properties were investigated by Open-circuit potential measurement (OCP) under a 500 W xenon lamp (CHF-XM-500W, Beijing Trusttech Co. Ltd.).

Fabrication of the $MoSe_2$–rGO/PI Composite Film: $MoSe_2$ was carried out at a potential of –0.6 V in a solution containing 0.04 M Na_2MoO_4, 0.02 M H_2SeO_3, and 0.2 M NaAc–HAc buffered solution on substrate rGO/PI in a conventional three-electrode. Here, the rGO/PI substrate acts as the working electrode with the area of 0.1256 cm^2; it was synthesized according to previous work,[42] the only difference was that 0.0769 g (15 wt%) rGO was added to enhance the conductivity of the material in this work. A Pt wire and a saturated calomel electrode (SCE) were used as counter and reference electrode. These electrodes were connected to a CHI 832 electrochemical workstation. All the chemicals were of analytical grade. All the aqueous solution were made up of water purified by Milli–Q pure water system (Millipore, electrical resistivity 18.2 MΩ cm^{-1}).

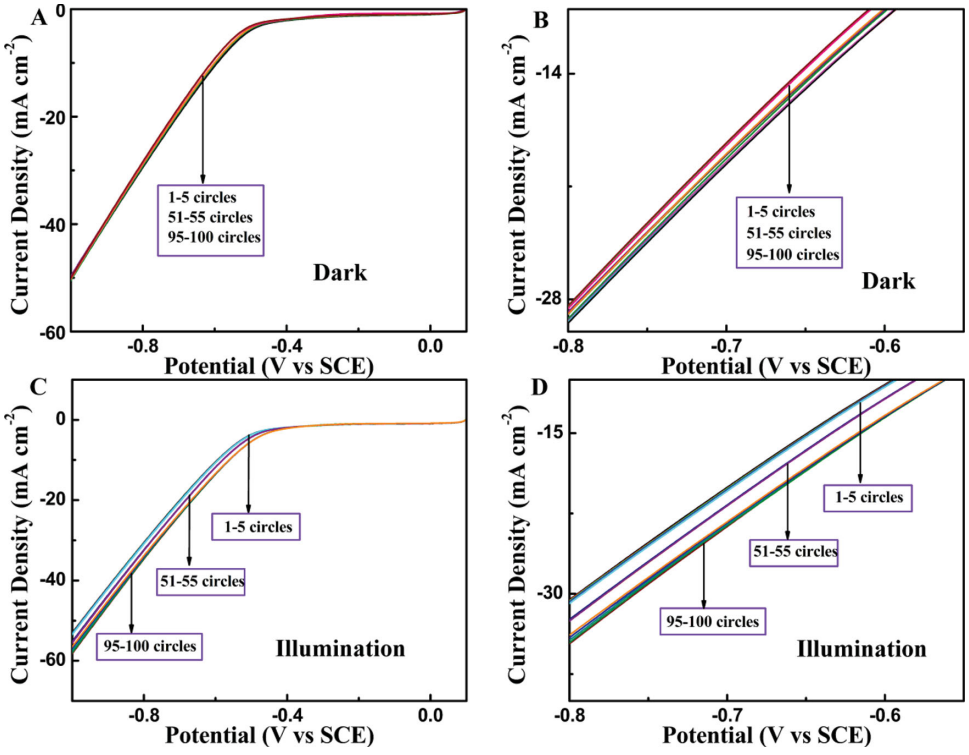

Figure 9. Catalyst stability tests for $MoSe_2$ with 100 cycles: A,B) in the dark and C,D) under illumination.

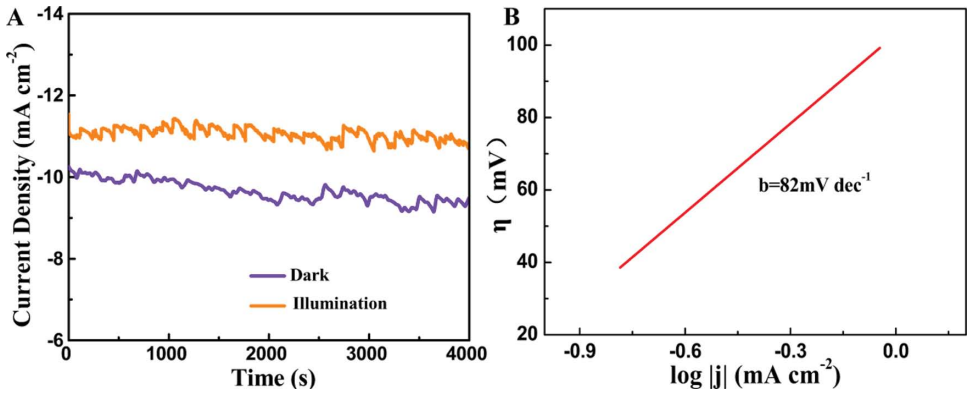

Figure 10. A) Plot of cathodic dark current at –0.6 V vs SCE, B) Tafel plots of $MoSe_2$–rGO/PI film.

Acknowledgements

This work is supported by the National Natural Science Foundation of China (Grant Nos. 51372106).

Received: June 4, 2014
Revised: July 14, 2014
Published online: September 5, 2014

[1] M. S. Dresselhaus, I. L. Thomas, *Nature* **2001**, *414*, 332.
[2] T. R. Cook, D. K. Dogutan, S. Y. Reece, Y. Surendranath, T. S. Teets, D. G. Nocera, *Chem. Rev.* **2010**, *110*, 6474.
[3] J. R. McKone, E. L. Warren, M. J. Bierman, S. W. Boettcher, B. S. Brunschwig, N. S. Lewis, H. B. Gray, *Energy Environ. Sci.* **2011**, *4*, 3573.
[4] J. R. McKone, A. P. Pieterick, H. B. Gray, N. S. Lewis, *J. Am. Chem. Soc.* **2013**, *135*, 223.
[5] M. A. Lukowski, A. S. Daniel, F. Meng, A. Forticaux, L. Li, S. Jin, *J. Am. Chem. Soc.* **2013**, *135*, 10274.
[6] Y. F. Shi, C. X. Hua, B. Li, X. P. Fang, C. H. Yao, Y. C. Zhang, Y. S. Hu, Z. X. Wang, L. Q. Chen, D. Y. Zhao, G. D. Stucky, *Adv. Funct. Mater.* **2013**, *23*, 1832.
[7] S. M. Delphine, M. Jayachandran, C. Sanjeeviraja, *Crystallogr. Rev.* **2011**, *17*, 281.
[8] P. P. Hankare, A. A. Patil, K. M. Garadkar, D. J. Sathe, A. H. Manikshete, I. S. Mulla, *J. Cryst. Growth* **2008**, *311*, 15.
[9] H. T. Wang, D. Kong, P. Johanes, J. J. Cha, G. Y. Zheng, K. Yan, N. Liu, Y. Cui, *Nano Lett.* **2013**, *13*, 3426.
[10] D. Kong, H. Wang, J. J. Cha, M. Pasta, K. J. Koski, J. Yao, Y. Cui, *Nano Lett.* **2013**, *13*, 1341.
[11] H. Tang, K. P. Dou, C. C. Kaun, Q. Kuang, S. Yang, *J. Mater. Chem. A.* **2014**, *2*, 360.
[12] X. L. Wang, Y. J. Gong, G. Shi, W. L. Chow, K. Keyshar, G. Ye, R. Vajtai, J. Lou, Z. Liu, E. Ringe, B. K. Tay, P. M. Ajayan, *ACS Nano* **2014**, *8*, 5125.
[13] S. Peulon, D. Lincot, *Adv. Mater.* **1996**, *8*, 166.
[14] B. M. Quinn, C. Dekker, S. G. Lemay, *J. Am. Chem. Soc.* **2005**, *127*, 6146.
[15] F. Endres, M. B. Dipl.-Chem, R. Hempelmann, H. Natter, *Angew. Chem. Int. Ed.* **2003**, *42*, 3428.
[16] J. A. Switzer, H. M. Kothari, P. Poizot, S. Nakanishi, E. W. Bohannan, *Nature* **2003**, *425*, 490.
[17] E. J. Menke, M. A. Thompson, C. Xiang, L. C. Yang, R. M. Penner, *Nat. Mater.* **2006**, *5*, 914.
[18] C. Fan, Z. M. Wei, S. X. Yang, J. B. Li, *RSC Adv.* **2014**, *4*, 775.
[19] M. Yoonessi, Y. Shi, D. A. Scheiman, M. L. Colon, D. M. Tigelaar, R. A. Weiss, M. A. Meador, *ACS Nano* **2012**, *6*, 7644.
[20] D. Chen, H. Zhu, T. X. Liu, *ACS Appl. Mater. Interfaces* **2010**, *2*, 3702.
[21] J. Longun, J. O. Iroh, *Carbon* **2012**, *50*, 1823.
[22] S. Murugesan, A. Akkineni, B. P. Chou, M. S. Glaz, D. A. Vanden Bout, K. J. Stevenson, *ACS Nano* **2013**, *7*, 8199.
[23] X. L. Zheng, J. B. Xu, K. Y. Yan, H. Wang, Z. L. Wang, S. H. Yang, *Chem. Mater.* **2014**, *26*, 2344.
[24] Y. Liu, Y. X. Yu, W. D. Zhang, *J. Phys. Chem. C.* **2013**, *117*, 12949.
[25] W. Abdallah, A. E. Nelson, *J. Mater. Sci.* **2005**, *40*, 2679.
[26] J. Pouzet, J. C. Bernede, *Rev. Phys. Appl.* **1990**, *25*, 807.
[27] X. Fan, X. M. Meng, X. H. Zhang, M. L. Zhang, J. S. Jie, W. J. Zhang, C. S. Lee, S. T. Lee, *J. Phys. Chem. C* **2009**, *113*, 834.
[28] J. Kim, S. Byun, A. J. Smith, J. Yu, J. X. Huang, *J. Phys. Chem. Lett.* **2013**, *4*, 1227.
[29] Y. G. Li, H. L. Wang, L. M. Xie, Y. Y. Liang, G. S. Hong, H. J. Dai, *J. Am. Chem. Soc.* **2011**, *133*, 7296.
[30] Z. B. Chen, D. Cummins, B. N. Reinecke, E. Clark, M. K. Sunkara, H. F. Jaramillo, *Nano Lett.* **2011**, *11*, 4168.
[31] J. Baglio, G. Calabrese, D. Harrison, E. Kamieniecki, A. Ricco, M. Wrighton, G. Zoski, *J. Am. Chem. Soc.* **1983**, *105*, 2246.
[32] J. R. McKone, N. S. Lewis, H. B. Gray, *Chem. Mater.* **2014**, *26*, 407.
[33] W. Kautek, J. Gobrecht, H. B. Gerischer, *Phys. Chem.* **1980**, *84*, 1034.
[34] A. L. Linsebigler, G. Lu, J. T. Yates Jr, *Chem. Rev.* **1995**, *95*, 735.
[35] S. C. Moon, Y. Matsumura, M. Kitano, M. Matsuoka, M. Anpo, *Res. Chem. Intermed.* **2003**, *29*, 233.
[36] R. Molinari, T. Marino, P. Argurio, *Int. J. Hydrogen Energy* **2014**, *39*, 7247.
[37] T. J. Jacobsson, V. Fjällström, M. Edoff, T. Edvinsson, *Energy Environ. Sci.* **2014**, *7*, 2056.
[38] B. E. Conway, B. V. Tilak, *Electrochim. Acta* **2002**, *47*, 3571.
[39] N. Pentland, J. O. M. Bockris, E. Sheldon, *J. Electrochem. Soc.* **1957**, *104*, 182.
[40] B. Hinnemann, P. G. Moses, J. Bonde, K. P. Jorgensen, J. H. Nielsen, S. Horch, I. Chorkendorff, J. K. Norskov, *J. Am. Chem. Soc.* **2005**, *127*, 5308.
[41] C. Xu, S. J. Peng, C. L. Tan, H. X. Ang, H. T. Tan, H. Zhang, Q. Y. Yan, *J. Mater. Chem. A* **2014**, *2*, 5597.
[42] Y. M. Jiang, L. P. Jia, S. J. Yu, C. M. Wang, *J. Mater. Chem. A* **2014**, *2*, 6656.